JAMSTEC Report of Research and Development, Volume 6, November 2007, 21–30

Ocean surface albedo in AFES

Takeshi Enomoto[1]

Abstract The albedo of the ocean surface is of primary importance in the radiative energy balance of the Earth. It takes the smallest value of close to 0 over ocean water and the largest value of nearly 1 over snow-covered sea ice. The albedo of ocean water is determined by of the solar zenith angle, slope of the surface and optical properties of the atmosphere and ocean. The albedo of sea ice is significantly influenced by snow cover. During the warm season, ponds of melt water of snow and ice result in large reduction of albedo. Based on the knowledge from foregoing observational and modelling studies, the treatment of the ocean surface albedo in AFES (atmospheric general circulation model for the Earth Simulator) has been improved. Recent modifications to albedo parametrizations incorporated in AFES are described and optimum values for various parameters are adjusted to the observation data. The effects of albedo on global energy balance and atmospheric circulation are discussed.

Keywords: radiative energy balance, solar zenith angle, snow cover, melt pond, parametrization

1. Introduction

There is a large contrast of albedo between ocean water ("black") and sea ice ("white"). Over open (unfrozen) ocean water, the most of the solar radiation is absorbed by the ocean. Over sea ice, especially when covered entirely with fresh snow, the most of solar radiation is reflected. Large variation implies a significant positive feedback on climate (sea ice-albedo feedback hypothesis[1)]). In the global atmospheric models, it is important to adequately reproduce such large variation of albedo over ocean since it is of primary importance on the global radiative energy budget. It is also important for reproducing correct local temperature near the surface.

In coupled atmosphere-ocean climate models, the solar energy input into ocean is determined by the ocean surface albedo. Erroneous values of albedo heat or cool the ocean and create biases in the sea-surface temperature (SST). The atmosphere then responds to the unrealistic SST distribution. As a result, errors in albedo lead to climate drift through atmosphere-ocean interactions. Therefore it is important to represent albedo and set values for parameters related to albedo carefully in order to improve the representation of the climate.

In this manuscript, recent modifications of in AFES (atmospheric general circulation model for the Earth Simulator)[2)3)4)] are described. Parametrizations of albedo of ocean water and sea ice are described in Section 2 and 3, respectively. In each of those section, the schemes used in other models are reviewed then the new implementation in AFES is described. In Section 4, the results of one-year integrations of AFES with and without changes in sea surface albedo are compared and final remarks are given.

2. Albedo of ocean water

2.1 Dependency to solar zenith angle

The reflection of the direct solar radiance incident to the smooth surface of water are described by Fresnel's law. The reflectances of the light perpendicular (s-polarized) and parallel (p-polarized) to the plane of incidence are

$$R_s = \left(\frac{\cos\theta_i - n\cos\theta_r}{\cos\theta_i + n\cos\theta_r}\right)^2, \quad R_p = \left(\frac{n\cos\theta_i - \cos\theta_r}{n\cos\theta_i + \cos\theta_r}\right)^2 \qquad (1)$$

respectively. Here θ_i and θ_r are the angle of incident and refraction and n is the refractive index. For the reflectance

1 The Earth Simulator Center, Japan Agency for Marine-Earth Science and Technology

of the unpolarized light is the mean of the two[5]. Figure 1 shows the albedo of the s- (solid curve) and p-polarized (broken curve) light and the mean of the two (dotted curve) with $n = 1.33$. The albedo is nearly constant until the solar zenith angle is below 60° but increases sharply between 60° and 90°. Schlick[6] proposed a faster approximation of the albedo of unpolarized light:

$$R = R_0 + (1 - R_0)(1 - \cos\theta)^5. \quad (2)$$

The line-dotted curve in Fig. 1 represents a case with $R_0 = 0.02$. This form is used for the ground albedo of snow and ice in MATSIRO[7].

Payne[8] conducted an observation of sea surface albedo at a fixed platform. Briegleb et al.[9] proposed the parametrization of the ocean surface albedo based on Payne's observation in the following form

$$\alpha(\mu) = \frac{0.026}{1.1\mu^{1.7} + 0.065} + 0.15(\mu - 1)(\mu - 0.5)(\mu - 1) \quad (3)$$

where α is the albedo and $\mu = \cos(\theta)$. This parametrization is used in Community Climate System Model Coupler[10].

Taylor et al.[11] proposed the following equation based on aircraft measurements and applied it to the United Kingdom Meteorological Office (UK MetOffice) Unified Forecast/Climate Model (UM)

$$\alpha(\mu) = \frac{0.037}{1.1\mu^{1.4} + 0.15}. \quad (4)$$

This form is also used in the European Centre for Medium-Range Weather Forecasts (ECMWF) Integrated Forecast System (IFS)[12].

Figure 2 compares the two parametrization schemes (Eq. (3) and (4)). The former is steeper and closer to the theoretical curve. The difference might have arisen from the condition of the sea surface measured during the observations that two parametrizations are based upon. One of the possible sources of difference is the wind speed. The larger the wind speed the sea surface is more tilted. When the sea surface is tilted the actual incident angle becomes smaller. As a result, the albedo become smaller. Dependency to the wind speed is discussed in the next subsection.

2.2 Dependency to wind speed and atmospheric optical depth

Hansen et al.[13] proposed the following formula to take the influence of the wind speed in to account.

$$\alpha(x, v_s) = 0.021 + 0.0421x^2 + 0.1283x^3 - 0.04x^4 + \frac{3.12x^5}{5.68 + v_s} + \frac{0.074x^6}{1 + 3v_s} \quad (5)$$

where $x = 1-\mu$. Figure 3 shows the albedo at different wind speeds calculated with Eq. 5. As discussed at the end of the last subsection, the albedo is subject to the influence of the wind speed, especially at large solar zenith angles, due to the slope of wave facets. A comparison between Fig. 2 and Fig. 3 indicates that the albedo parametrizations suggested by Briegleb et al.[9] (Eq. 3) and by Taylor et al.[11] (Eq. 4) correspond to weak and strong wind regimes in the parametrization by Hansen et al.[13] (Eq. 5).

Jin et al.[14] proposed a more comprehensive parametrization of ocean surface albedo. In their parametrization, the albedo depends upon the solar zenith angle, surface wind speed and atmospheric and oceanic optical depths. Look-up tables in terms of the four parameters are created using a coupled ocean-atmosphere radiative transfer code and validated against measurements at a sea platform. There are tables for 24 and 4 spectral bands and broadband available online. The broadband table is obtained and the dependencies of albedo upon the solar zenith angle, wind speed and atmospheric optical depth are examined. The oceanic optical depth, primarily determined by the Chlorophyll concentration, is not considered here but would be worthwhile to examine its impact with a atmosphere-ocean coupled model, such as CFES (coupled atmosphere-ocean general circulation model for the Earth simulator), with an marine biological model.

Figure 4 shows the variation of albedo with the solar zenith angle at different wind speeds without aerosols or clouds (the atmospheric optical depth is set to naught). The wind speed is varied between 0 and 10 ms^{-1} since Jin et al.[14] point out that the effects of foam becomes non negligible when the wind speed exceeds 15 ms^{-1}. The parametrization by Taylor et al.[11] agrees remarkably well with the values from the look-up table by Jin et al. [14] except that the former does not include the effect of the wind speed.

When typical values of aerosols and clouds are provided to the look-up table, the albedo be-comes less sensitive to the solar zenith angle. In a case with the atmospheric optical depth of 1, representing a value over ocean due to sea salt, the albedo at low sun is much smaller (Figure 5a). With a larger optical depth representing an overcast condition by clouds (Fig. 5b), the albedo does not depend upon the solar zenith angle in this case due to the relative increase of diffused light. Moreover, the difference among various wind speeds is very small.

2.3 Modifications in AFES

The modifications to AFES is as follows. The effect of the solar zenith angle is incorporated by adopting Taylor et al.[11] The dependencies to the surface wind speed and Chlorophyll concentration are not implemented at this

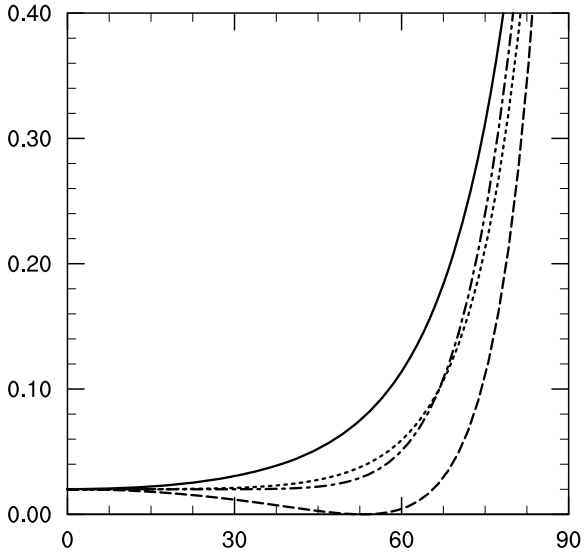

Figure 1: The albedo of the smooth water surface described by Fresnel's law of reflection and its approximation. The solid, dashed and dotted curves represent the albedo of s-, p-polarized and unpolarized light, respectively. The dash-dotted curve represents the approximation of the albedo of unpolarized light by Schlick (1992)[3].The refractive index of water (n = 1.33) is used in the calculation of the albedo.

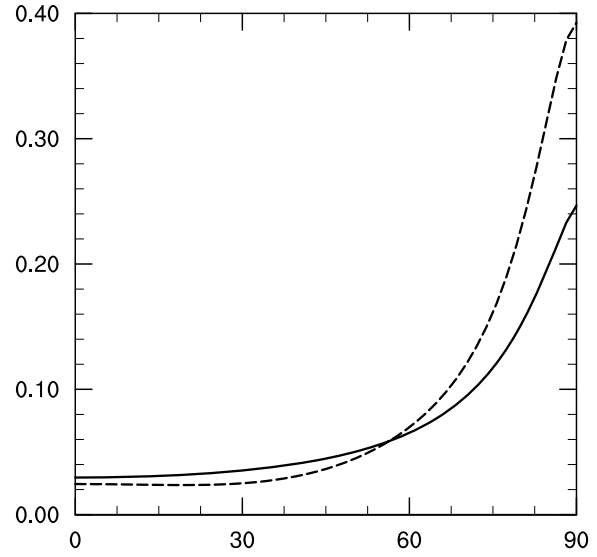

Figure 2: Parametrizations of the sea-surface albedo proposed by Briegleb et al.[9] (dotted curve) and Taylor et al.[10] (solid curve).

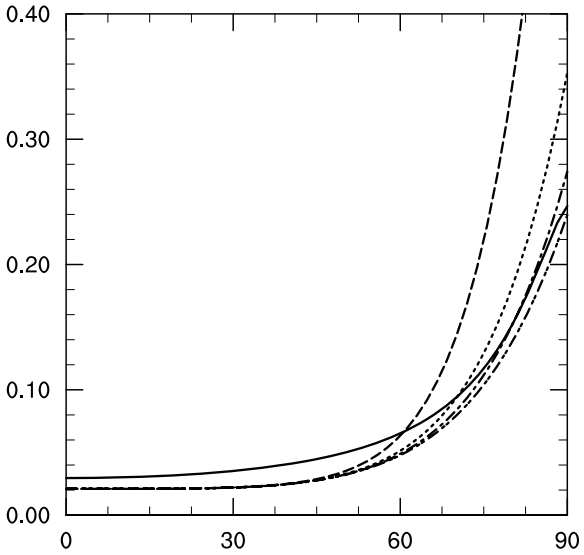

Figure 3: Albedos at different wind speeds in the parametrization proposed by Hansen et al.[13] The broken, dotted, dash-dotted and dash-two dotted curves represent the albedo at v_s = 0, 10, 20, 30 ms^{-1}. The albedo by Taylor et al.[11] is also drawn in the solid curve to for comparison.

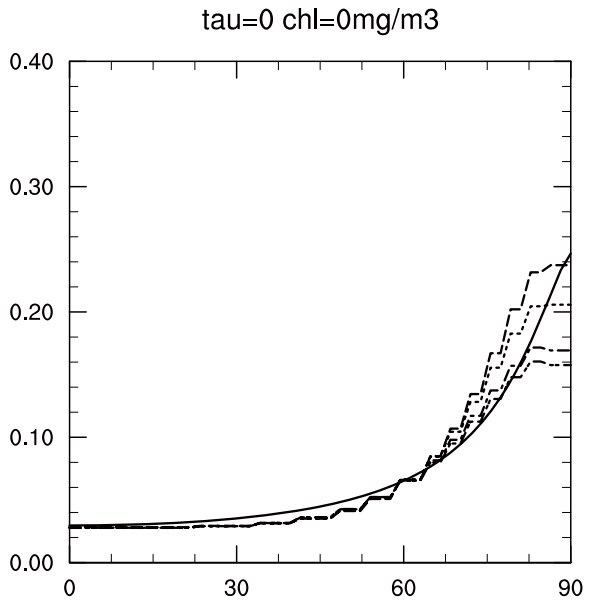

Figure 4: Albedos at different wind speeds in the parametrization proposed by Jin et al. [14] with the pristine atmosphere. The broken, dotted, dash-dotted and dash-two dotted curves represent the albedo at v_s = 0, 5, 10, 15 ms^{-1}. The albedo by Taylor et al.[11] is also drawn in the solid curve to for comparison.

point. The effect of atmospheric optical depth is introduced by separating direct and diffuse lights. The modified code make use of the feature of the radiation code[15)16)17)] to treat direct and diffused lights separately. The intensity of diffusion is determined by the aerosol and cloud water concentration. The constant value of 0.06 (0.07 previously for both direct and diffuse lights) is used for diffused light.

Test runs to validate the modifications have been conducted at a T119L48 (triangular truncation at wave number 119, corresponds to about 1° horizontal grid spacing and 48 vertical layers) resolution for one year from climatological conditions of 1 January, prepared from the European Centre for Medium-range Weather Forecasts (ECMWF) reanalysis 40 (ERA-40).[18)] The climatological sea surface temperature and sea ice distribution created from the optimum (OI) interpolation sea surface temperature (SST) and sea ice analysis version 2[19)] is used as the boundary forcings.

In AFES 2, a constant value of 0.07 has been used for both direct and diffuse lights. As a result the albedo is constant over ocean irrespective to variations of aerosols and clouds. With the introduction of the parametrization, the albedo not only varies with the solar zenith angle but also with atmospheric optical depth. Although the albedo increases at low sun, the incoming solar radiation at the sea surface increases in general due to a sightly smaller values at high sun for direct light and for diffuse light (Fig. 6). Larger values of the albedo in the case with the parametrization are found along the fringe of the sea ice in the winter hemisphere near the 60-degree latitudinal circle. Increase of insolation in the subtropics act to reduce the model bias. Although a change in radiative balance over the ocean is ineffective in the atmosphere-only simulations where the sea surface temperature is imposed, it might be significant in the coupled atmosphere-ocean simulations since the albedo determines the portion of solar energy input into the ocean.

3. Albedo of sea ice

3.1 Parametrizations of sea ice albedo

Primary factors that influence the albedo of the ocean with sea ice are its concentration (open lead fraction), snow cover, and melt pond fraction. Parametrizations of sea ice albedo are built to represent some or all of those factors. In this section, the sea ice albedo parametrization in three atmospheric models are described.

a) *HIRAM*. The original sea ice parametrization of a regional climate model HIRHAM is[20)]

$$\begin{aligned} \alpha &= 0.75 && T_s \le 271.65\mathrm{K} \\ \alpha &= 0.75 + 0.133(271.65 - T_s) && T_s > 271.65\mathrm{K} \end{aligned} \qquad (6)$$

where T_s is the surface temperature. This parametrization

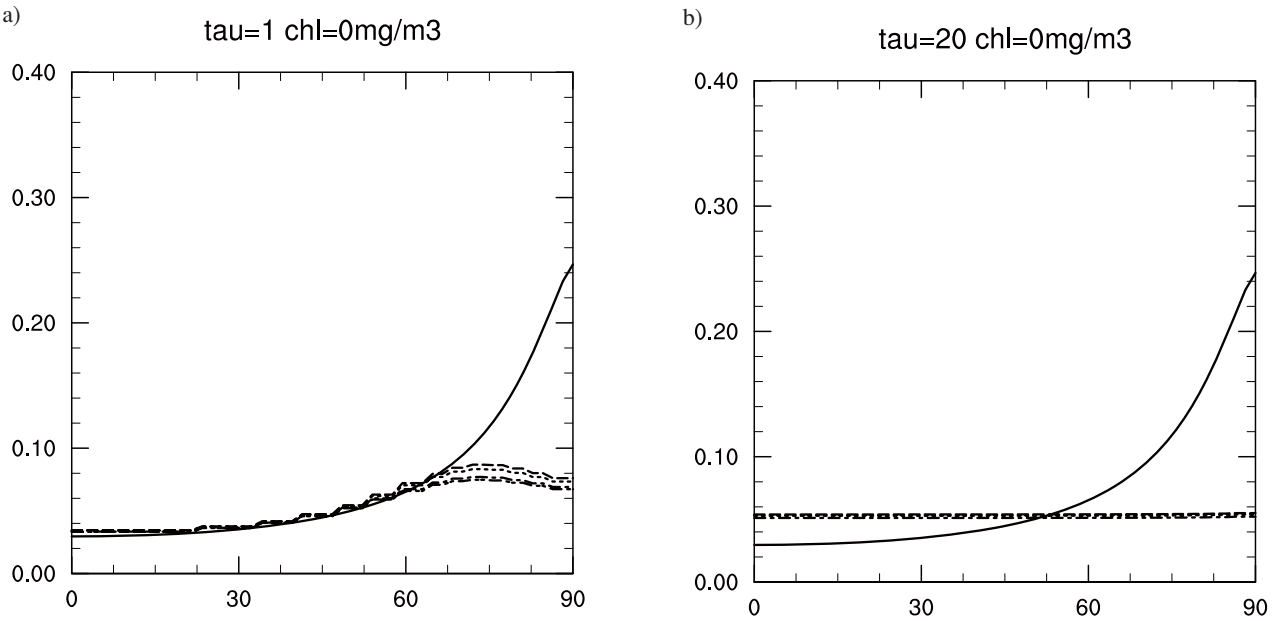

Figure 5: Albedos at different wind speeds in the parametrization proposed by Jin et al. [14)] with atmospheric optical depth of 1 (Panel a) and 20 (Panel b). The broken, dotted, dash-dotted and dash-two dotted curves represent the albedo at v_s = 0, 5, 10, 15 ms^{-1}. The albedo by Taylor et al.[11)] is also drawn in the solid curve to for comparison.

a)

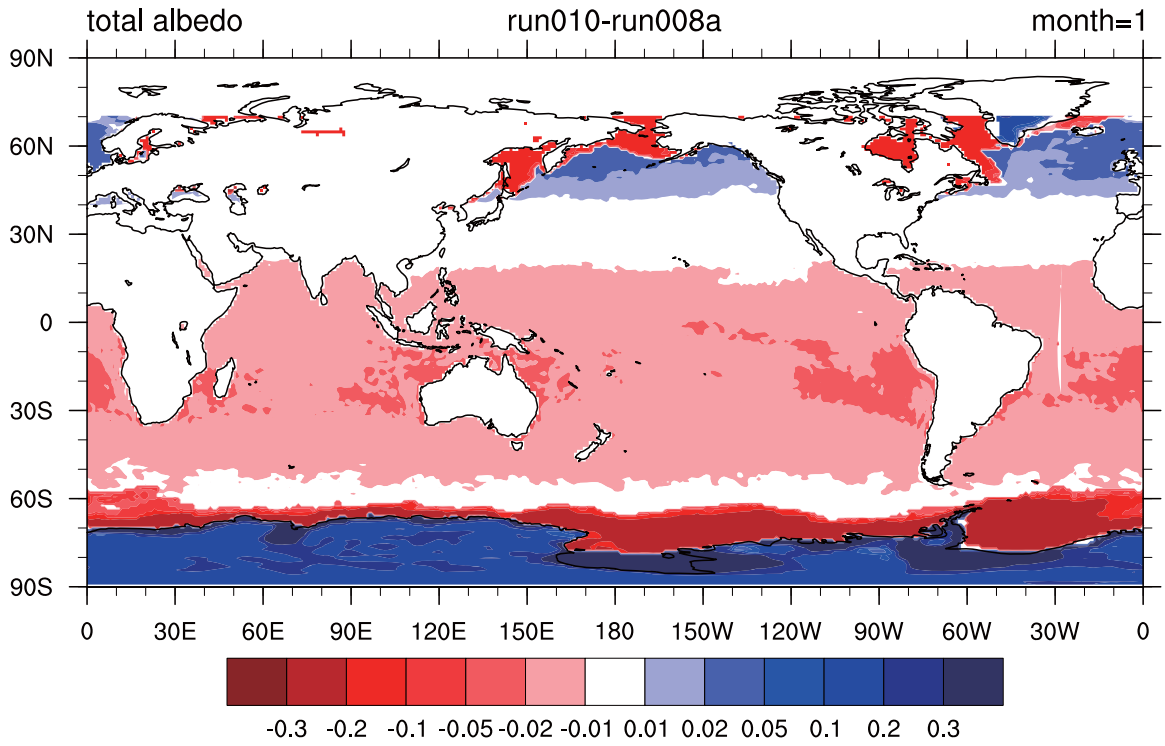

b)

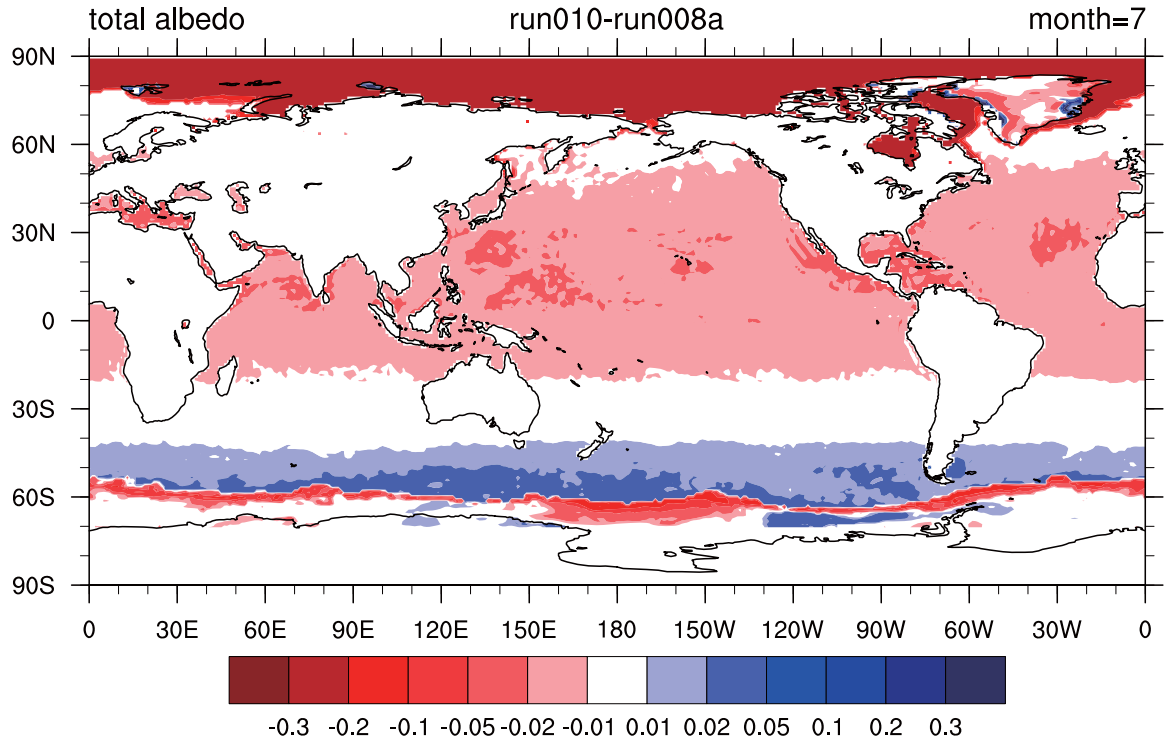

Figure 6: The difference of the monthly mean albedos in January (Panel a) and in July (Panel b) between the simulations using AFES with the parametrization by Taylor et al.[11] and with a constant value (the former minus the latter). Large difference in the polar region in the summer is due to the different settings in snow and ice.

is improved by Kølzow et al.[20] to include effects of the snow cover and melt pond fraction.

$$\alpha = f_s\alpha_s + (1 - f_s)[(1 - f_p)\alpha_i + f_p\alpha_p] \quad (7)$$

where f_s and f_p represents the snow cover and melt pond fraction, respectively and α_s, α_i, α_p the snow, ice and melt pond albedos, respectively. The values of snow and ice albedos are as follows: α_s = 0.84 and 0.77 for dry and melting snow, respectively and α_i = 0.57 and 0.51 for dry and melting bare sea ice. For the $T_s > T_c$ = 2 °C, the albedo and fraction of the melt pond are given by

$$\alpha_p = 0.36 - 0.1(T_s - T_c), \quad (8)$$

$$f_p = 0.11(T_s - T_c), \quad (9)$$

b) CAM. The sea ice albedo scheme in the National Center for Atmospheric Research (NCAR) Community Atmosphere Model (CAM)[21] does not have melt pond effects but distinguishes the visual (VIS) and near-infrared (NIR) wave lengths. When $T_s > T_c$ = –1 °C, the snow and ice albedos are modified from the minimum values

$$\begin{aligned} \alpha_s &= \alpha_{s\,\min} - a_s(T_s - T_c) \\ \alpha_i &= \alpha_{i\,\min} - 0.075(T_s - T_c) \end{aligned} \quad (10)$$

In CAM 2, $\alpha_{s\,\min}$ = 0.98 and 0.70, α_s = 0.1 and 0.15, $\alpha_{i\,\min}$ = 0.78 and 0.36 for VIS and NIR, respectively. The snow and ice albedos are combined by Eq. 7 with f_p = 0. Slightly smaller values for albedos are used in CAM 3, but the values used in CAM 2 fit better with the observed values of albedo in the Surface Heat Budget of Arctic Ocean (SHEBA) project.[22]

c) AFES. The snow albedo in AFES is linearly interpolated between the dry and wet values α_{sd} = 0.8 and α_{sw} = 0.6, respectively when $T_d < T_s < T_w$. The default values of dry and wet threshold tempera-ture are T_d = –15 °C and T_w = 0 °C, respectively.

$$\alpha_s = \alpha_{sw} + \frac{\alpha_{sd} - \alpha_{sw}}{T_d - T_w}(T_s - T_w) \quad (11)$$

The default value of the ice albedo is α_{id} = 0.6. In order to roughly represent melt ponds, a smaller value of α_{iw} = 0.5 is used for ice when $T_s > T_c$ = –1.01 °C. The snow and ice albedos are averaged with the snow cover as a weight by Eq. 7 with f_p = 0.

3.2 Validations against the SHEBA dataset

Using the three parametrizations described in the previous subsection, the sea ice albedo at the SHEBA site from April to September is simulated and compared with the tower and line observations (Fig. 7). Open leads were not found along the albedo line.[22] The snow cover (dashed curve) is assumed to decrease from 1 to 0 in June as in Køltzow et al.[20] During the winter and spring when the surface is snow covered the albedo is spatially homogeneous. As the snow melts, the surface is a mixture of snow, bare ice and melt ponds and the albedos become highly variable. Therefore, in cold seasons, the tower albedo (thin black curve) can represent the spatial average at the SHEBA site. In warm seasons, however, the albedo measured along the 200-m length line (thick black curve) better represents the spatial average. The spectral albedo used in CAM is converted to the broadband value by the following weights.

$$\alpha_{BB} = 0.53\alpha_{VIS} + 0.47\alpha_{NIR}. \quad (11)$$

In the melting snow stage, the weighed average between the snow and ice albedos can ef-fectively represent the reduction in CAM (blue) and AFES (green). The original parametrization in HIRHAM (red) is unable to represent such a reduction. It fluctuates between large and small values depending on the input surface temperature. The default values of snow and ice albedo in AFES seem to be too small.

In order to correctly represent the drop to α = 0.4 in the summer, the melt pond parametrization (Eq. 7–9) is applied to HIRHAM and CCSM. The improved HIRHAM's parametrization distinguishes the snow and ice albedo. The values of dry and wet snow, dry and wet sea ice albedo are 0.84, 0.77, 0.57 and 0.51, respectively. With the melt pond parametrization, smaller values in the summer are reproduced. However, the seasonal development of melt ponds is not necessarily captured as will be discussed later.

In the modified version used in AFES, the values of snow albedos are increased and those for sea ice are slightly decreased to better fit the SHEBA data. Distinction between VIS and NIR albedos is introduced. The same values for dry and wet snow and dry sea ice as those used in CAM are adopted. They are very close to the broadband values used in the modified version of HIRHAM's albedo parametrization. The spectral value for the wet sea ice is determined as follows. The average melt pond fraction of 0.3 is assumed and the melt pond albedo of 0.3 for VIS and 0.06 for IR are used based on the observation by Perovich et al.[22] Table 1 summarizes the new

Table 1: The new and old albedos for snow and sea ice for AFES.

	VIS	NIR	BB	old
Dry snow	0.98	0.7	0.85	0.8
Wet snow	0.90	0.60	0.76	0.6
Dry sea ice	0.78	0.36	0.58	0.8
Wet sea ice	0.63	0.27	0.46	0.5

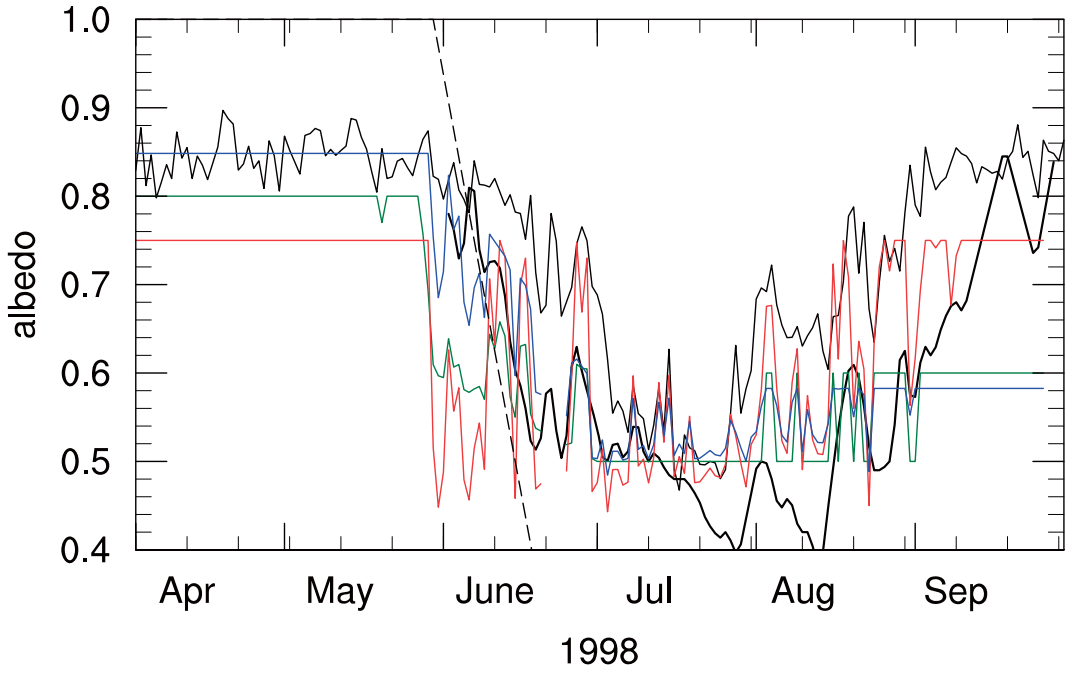

Figure 7: Albedos observed at the SHEBA site[22] and simulated using three sea ice albedo parametrizations. The thin and thick black curves represent tower and line observations. The red, blue and green curves are simulated values using the sea ice parametrizations in HIRHAM, CAM and AFES, respectively. The dashed line is an assumed snow cover.

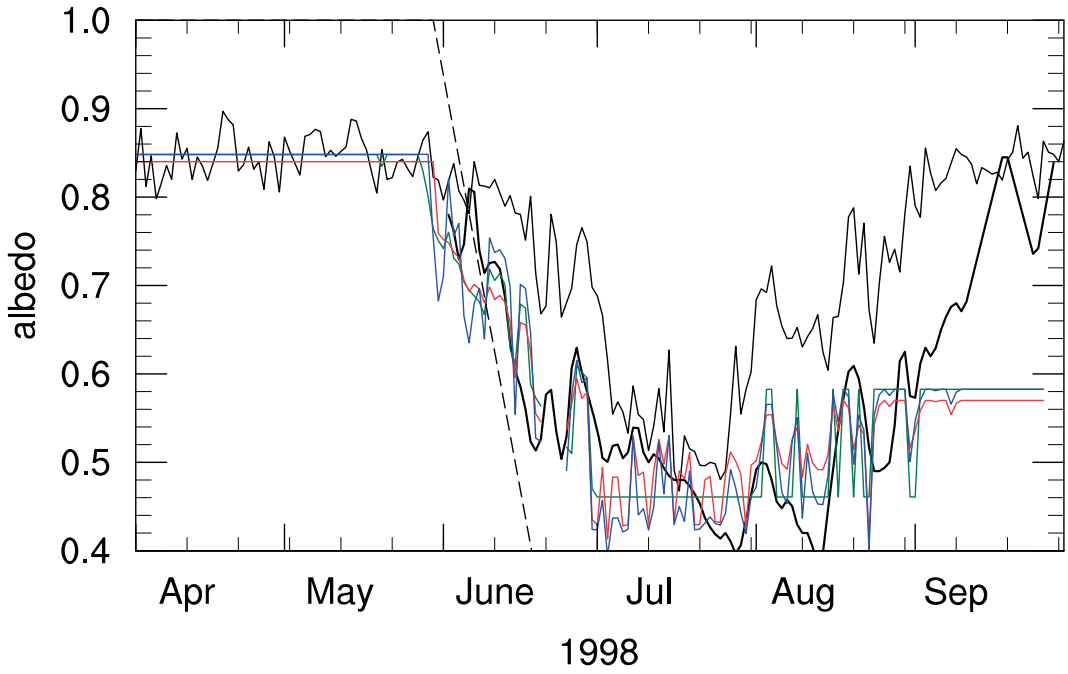

Figure 8: Albedos observed at the SHEBA site[22] and simulated using three modified version of the sea ice albedo parametrizations. The thin and thick black curves represent tower and line observations. The red, blue and green curves are simulated values using the modified version of the sea ice parametrizations in HIRHAM, CAM and AFES, respectively. The dashed line is an assumed snow cover.

values of the spectral and broadband albedos and the old broad band values for snow and sea ice.

Figure 8 shows the albedo simulations using modified parametrizations of HIRHAM (red), CCSM (blue), and AFES (green). The former two use the melt pond parametrization (Eq. 7–9). With the modified versions, three parametrizations result in values very close to the observations. In HIRAM and AFES, the bias in the spring is removed mainly by using the snow cover and optimized albedo for snow and ice, respectively. In HIRAM and CCSM, the melt pond parametrization effectively lower the albedo during the summer. In AFES, the same improvement is achieved by reducing the value to the wet ice albedo. The three parametrizations, however, share a common weakness. They all give too small a value in early summer. Thus the time evolution of the albedo at intra-seasonal time scales is not reproduced well. The melt pond parametrization rather introduces fluctuation at the day-to-day scale, which might be noise than signal. For this reason, the melt pond parametrization is not adopted in AFES.

4. Summary and Discussions

The new parametrizations of the sea surface albedo implemented in AFES are as follows. Over the ocean water, the zenith angle dependency has been introduced. At small zenith angles, the albedo takes smaller values in the new scheme. As a result short wave insolation increased in tropics and subtropics. The direct and diffuse lights are distinguished. For the frozen ocean, the albedos for snow and ice are tuned to the values suggested in observational studies and validated with the SHEBA data sets. The visual and near-infrared bands are distinguished in the new scheme.

In the new set of values, the contrast between snow and ice albedos has been increased. This change has impact on climate in polar regions, especially in terms of the near-surface temperature. Figure 9 shows the 2-m temperature averaged for March-April-May (MAM) in the simulations without and with the initial snow distribution. two simulations. Over the sea ice, a uniform value of 100 kg m^{-2} of snow that corresponds to 100 % snow cover at the initial date of 1 January is assumed. The difference is more conspicuous in the spring than in the winter due to the lack of the insolation in the polar region during the winter. In the simulation without the initial snow, the near-surface temperature in the Arctic Sea is unrealistically warmer than the surrounding continents and islands.

The importance of the initial snow distribution is obviously important for seasonal scale simulations. Over land in the Northern Hemisphere, snow analysis is available. Over the sea ice, which occupies the Arctic region, data is not readily available. With the reasonable values of the albedos for snow and ice, the lack of snow at the initial time could cause a serious error in weather forecast. An artificially large albedo for sea ice used to represent the snow could also cause a large error in the summer over the multi-year ice. Although the initial conditions are less important in the simulations for decades, a longer spin up might be required without a realistic snow distribution at the initial time. The simulated snow amount significantly affects the climate and seasonal cycle.

The modifications of AFES discussed here are automatically reflected in CFES. For example, the introduction of the solar zenith angle dependency diminishes the cool bias found in the sea-surface temperature (SST) in the subtropics and tropics. The parameters of snow and ice albedos determined for AFES can be used in CFES as well.

In determining the values of the albedos, the SHEBA data sets have been quite useful. There are still many uncertainties associated with sea ice: the snow distribution over sea ice as discussed above, melt pond and lead fractions and the aerodynamic roughness of the sea ice. The parametrization of the albedo of the ocean water is not yet robust, especially at high wind. The observations targeted to reduce the model bias over sea ice would be very helpful in the improvement of weather and climate models.

References

1) J.A. Curry and J.L. Schramm, “Sea ice-albedo climate feedback mechanism”, J. Climate, 8, 240–247 (1995).

2) S. Shingu, H. Fuchigami, M. Yamada, “Vector parallel programming and performance of a spectral atmospheric model on the Earth Simulator”, in Realizing Teracomputing: Proceedings of the Tenth ECMWF Workshop on the Use of High Performance Computing in Meteorology, W. Zwieflhofer and N. Kreitz (Eds.), World Scientific, 29--46 (2003).

3) W. Ohfuchi, H. Nakamura, M. K. Yoshioka, T. Enomoto, K. Takaya, X. Peng, S. Yamane, T. Nishimura, Y. Kurihara, and K. Ninomiya “10-km mesh meso-scale resolving simulations of the global atmosphere on the Earth Simulator: Preliminary outcomes of AFES (AGCM for the Earth Simulator)”, J. Earth Simulator, 1, 8–34 (2004).

4) T. Enomoto, A. Kuwano-Yoshida, N. Komori, and W. Ohfuchi. “Description of AFES 2: improvements for high-resolution and coupled simulations”, in High Resolution Numerical Mod-elling of the Atmosphere and Ocean. W. Ohfuchi and K. Hamilton (eds), Springer, New York, in press.

5) F.A. Jenkins and H.E. White, Fundamentals of Optics fourth edition (McGraw-Hill, 1981).

6) C. Schlick, “Divers élémants pour la synthèse d’images réalistes”, Ph.D thesis, Université Bor-deaux 1, (1992), in French.

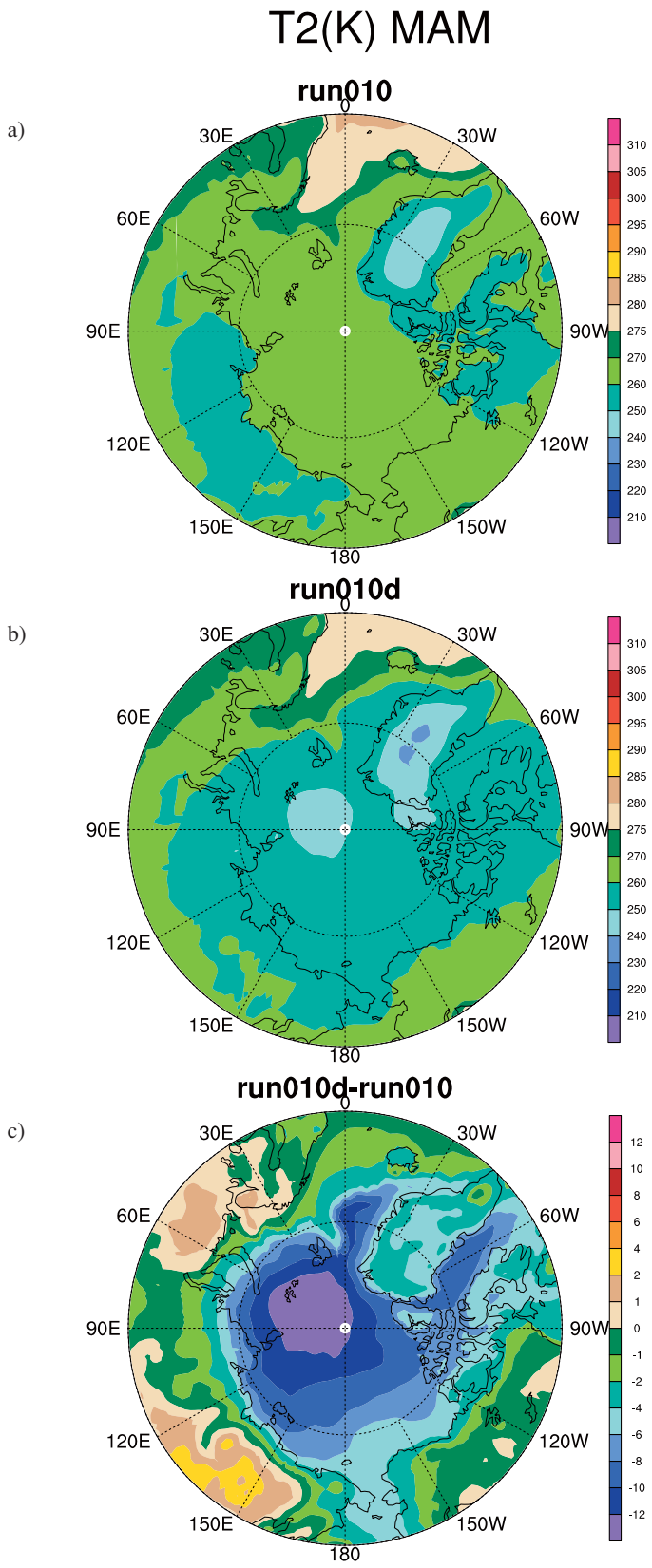

Figure 9: March-April-May averages of the 2-m temperature in the simulations a) without and b) with the initial snow distribution in the Northern Hemisphere. Panel c) shows the difference (b–c).

7) K. Takata, S. Emori, T. Watanabe, "Development of the minimal advanced treatments of surface tnteraction and runoff", Global and Planetary Change, 38, 209–222 (2003).
8) R.E. Payne, "Albedo of the sea surface", J. Atmos. Sci., 29, 959–970 (1972).
9) B.P. Briegleb, P. Minnis, V. Ramanathan and E. Harrison, "Comparison o f regional clear-sky albedos inferred from satellite observation and model computations", J. Clim. Appl. Meteorol. 25, 214–224 (1986).
10) The CCSM coupler version 6.0 Documentation, the CCSM project (2004).
11) J.P. Taylor, J. M. Edwards, M.D. Glew, P. Hignett and A. Slingo, "Studies with a flexible new radiation code. II: comparisons with aircraft short-wave observations", Quart. J. Roy. Meteor. Soc., 122, 839–861 (1996).
12) IFS documentation CY28r1, the European Centre for Medium-Range Weather Forecasts (2004).
13) J. Hansen, G. Russell, D. Rind, P. Stone, A. Lacis, S. Lebedeff, R. Ruedy and L. Travis, "Efficient three-dimensional global models for climate studies: models I and II", Mon. Wea. Rev., 111(4), 609–662 (1983).
14) Z. Jin, T.P. Charlock, W.L. Smith Jr., and K. Rutledge, "A parameterization of ocean surface albedo", Geophys. Res. Lett., 31, L22301, doi:10.1029/2004GL021180 (2004).
15) T. Nakajima, M. Tsukamoto, Y. Tsuchima, A. Numaguti, and T. Kimura, Modeling of the radiative process in an atmospheric general circulation model. Appl. Opt., 39, 4869–4878 (2000).
16) M. Sekiguchi, T. Nakajima, K. Suzuki, K. Kawano, A. Higurashi, D. Rosenfeld, I. Sano, and S. Mukai, "Astudy of the direct and indirect effects of aerosols using global satellite data sets of aerosol and cloud parameters. J. Geophys. Rett., 108 (10.1029), 2002JD003359 (2003).
17) M. Sekiguchi, "A Study on evaluation of the radiative flux and its computational optimization in the gaseous absorbing atmosphere", Science Doctoral Dissertation, the University of Tokyo, 121pp (in Japanese), (2004).
18) S. M. Uppala, P. W. Kallberg, A. J. Simmons, U. Andrae, V. da Costa Bechtold, M. Fiorino, J. K. Gibson, J. Haseler, A. Hernandez, G. A. Kelly, X. Li, K. Onogi, S. Saarinen, N. Sokka, R. P. Allan, E. Andersson, K. Arpe, M. A. Balmaseda, A. C. M. Beljaars, L. van de Berg, J. Bidlot, N. Bormann, S. Caires, F. Chevallier, A. Dethof, M. Dragosavac, M. Fisher, M. Fuentes, S. Hagemann, E. Holm, B. J. Hoskins, L. Isaksen, P. A. E. M. Janssen, R. Jenne, A. P. McNally, J. Mahfouf, J. Morcrette, N. A. Rayner, R. W. Saunders, P. Simon, A. Sterl, K. E. Trenberth, A. Untch, D. Vasiljevic, P. Viterbo and J. Woollen, "The ERA-40 reanalysis", Quart. J. Roy. Meteor. Soc, 131, 2961–3012 (2005).
19) R. W. Reynolds, N. A. Rayner, T. M. Smith, D. C. Stokes and W. Wang, "An improved in situ and satellite SST analysis for climate", J. Climate, 15, 1609–1625 (2002).
20) M. Kølzow, S. Eastwood and J.E. Haugen, "Parameterization of snow and sea ice in climate models", Research Report no. 149, Norwegian Meteorological Institute, 37pp (2003).
21) W.D. Collins,P.J. Rasch, B.A. Boville, J.J. Hack, J.R. McCaa, D.L. Williamson, J.T. Kiehl, B. Briegleb,, "Description of the NCAR Community Atmosphere Model (CAM 3.0)", NCAR Technical Note, NCAR/TN-646+STR, 214 pp (2004).
22) D.K. Perovich, T.C. Grenfell, B. Light, P.V. Hobbs, "Seasonal evolution of the albedo of multiyear Arctic sea ice", J. Geophys. Res., 107(C10), 8044, doi:10.1029/2000JC000438 (2002).

(Received July 7, 2007)